lubricants

MDPI

Article

Physical Analysis of Thermophoresis and Variable Density Effects on Heat Transfer Assessment along a Porous Stretching Sheet and Their Applications in Nanofluid Lubrication

Zia Ullah [1,*] and Musaad S. Aldhabani [2]

[1] Department of Mathematics and Statistics, Sargodha-Campus, The University of Lahore, Sargodha 40100, Pakistan
[2] Department of Mathematics, Faculty of Science, University of Tabuk, P.O. Box 741, Tabuk 71491, Saudi Arabia; maldhabani@ut.edu.sa
* Correspondence: ziakhan.uos.72@gmail.com

Abstract: Nanofluids are engineered colloidal suspensions of nanoparticles in the base fluids. At very low particle concentration, nanofluids have a much higher and strongly temperature-dependent thermal conductivity, which enables them to enhance the performance of machining applications such as the cooling and lubrication of the cutting zone during any machining process, the vehicle's braking system, enhanced oil recovery (EOR), engine oil, and the drilling process of crude oil. In the current work, the density is assumed as an exponential function of temperature due to larger temperature differences. The main focus of this mechanism is the variable density effects on heat and mass characteristics of nanoparticles across the stretching porous sheet with thermophoresis and Brownian motion to reduce excessive heating in high-temperature systems. This is the first temperature-dependent density problem of nanofluid across the stretching surface. The coupled partial differential equations (PDEs) of the present nanofluid mechanism are changed into nonlinear coupled ordinary differential equations (ODEs) with defined stream functions and similarity variables for smooth algorithm and integration. The changed ODEs are again converted in a similar form for numerical outcomes by applying the Keller Box approach. The numerical outcomes are deduced in graphs and tabular form with the help of the MATLAB (R2013a created by MathWorks, Natick, MA, USA) program. In this phenomenon, the velocity, temperature, and concentration profile, along with their slopes, have been plotted for various parameters pertaining to the current issue. The range of parameters has been selected according to the Prandtl number $0.07 \leq Pr \leq 70.0$ and buoyancy parameter $0 < \lambda < \infty$, respectively. The novelty of the current work is its use of nanoparticle fraction along the porous stretching sheet with temperature-dependent density effects for the improvement of lubrication and cooling for any machining process and to reduce friction between tool and work piece in the cutting zone by using nanofluid. Moreover, nanoparticles can also be adsorbed on the oil/water surface, which alters the oil/water interfacial tension, resulting in the formation of emulsions.

Keywords: temperature-dependent density; nanofluid; Keller box method; porous medium; heat transfer; thermophoresis; stretching sheet; mass transfer

Citation: Ullah, Z.; Aldhabani, M.S. Physical Analysis of Thermophoresis and Variable Density Effects on Heat Transfer Assessment along a Porous Stretching Sheet and Their Applications in Nanofluid Lubrication. *Lubricants* **2023**, *11*, 172. https://doi.org/10.3390/lubricants11040172

Received: 6 March 2023
Revised: 31 March 2023
Accepted: 6 April 2023
Published: 10 April 2023

1. Introduction and Literature Review

The heat, mass, and momentum transfer in the laminar boundary layer nanofluid flow over a stretching porous sheet play an important theoretical and practical role in metallurgy and polymer technology. Nanofluids are suspensions of nanoparticles in fluids that show significant enhancement of their properties at modest nanoparticle concentrations. Engine oils, automatic transmission fluids, coolants, lubricants, and other synthetic high-temperature heat transfer fluids found in conventional truck thermal systems—e.g., radiators, engines, heating, ventilation, and air-conditioning—have inherently poor heat transfer properties. These could benefit from the high thermal conductivity offered by

nanofluids that resulted from the addition of nanoparticles. The results of previous research and field tests revealed that nanofluids could improve oil recovery through plugging and profile control, transformation of wettability of the rock surface, changes in oil–water interface properties, and increases in the viscosity ratio between fluids. On the other hand, nanoparticles might stabilize oil–water emulsions produced during the extraction stage, adversely affecting subsequent oil–water separation processes, especially electrical dehydration. Moreover, nanofluids have a much higher and strongly temperature-dependent thermal conductivity, which is considered to be a key parameter for enhanced performance for most of the machining applications. When nanoparticles are supplied along with base fluid, it comes with a ball bearing effect because of its nano size rang and the high thermal conducting nature of heat. Nanofluids proved themselves best as an option for any machining process as molybdenum disulfide nanoparticles, aluminum oxide nanoparticles, silver nanoparticles, graphite nanoparticles, and carbon nanotubes. The cooling of a sizable metallic plate across a stretching surface in a bath that may or may not contain an electrolyte poses a significant problem in a number of engineering processes, including extrusion, melt-spinning, hot rolling, wire drawing, the production of glass fiber, and the production of plastic/rubber sheets. In the manufacturing process, the production of polymer sheets and filaments are the most important factors. This kind of flow is used in many engineering processes, including plastic film stretching, continuous casting, glass fiber and paper production, food manufacturing, and the extrusion of polymers. It is helpful to leverage the combined effects of heat transmission and variable density to produce a finished product with the desired properties. Such factors are crucial, particularly in metallurgical processes that include the purifying of molten metal from non-metallic impurities and the cooling of continuous strips and filaments dragged through a quiescent fluid.

Enhanced oil recovery (EOR) has been widely used to recover residual oil after the primary or secondary oil recovery processes. Nanofluids have received extensive attention owing to their advantages of low cost, high oil recovery, and wide applicability. In recent years, nanofluids have been widely used in EOR processes. Moreover, several studies have focused on the role of nanofluids in the nanofluid EOR process. Nanofluids can alter the wettability of minerals (particle/surface micromechanics), oil/water interfacial tension (heavy oil molecules/water micromechanics), and structural disjoining pressure (heavy oil molecules/particle/surface micromechanics). They can also cause viscosity reduction (micromechanics of heavy oil molecules). Pourrajab and Noghrehabadi [1] illustrated bio convective mechanism of viscoelastic fluid across a stretched surface in a permeable material using kinetic temperature in the existence of a micro-organism. They found that conductivity and Reynolds ratio increase the temperature of fluid with decreasing behavior. Sarkar and Endalew [2] elaborated the impacts of the crystallization on viscoelastic small fluid particles with magnetohydrodynamic MHD (Magnetohydrodynamics is the study of the magnetic properties and behaviour of electrically conducting fluids) flow in porous material. They observed that the thickness of the temperature field decreases due to the maximum value of the Nusselt number. Kalavathamma and Lakshmi [3] studied the impact of various characteristics on the mass and heat transfer of viscous fluid particles across a horizontal cylinder saturated by permeable material. They found that the temperature distribution of the fluid decreases as the value of the Brownian motion parameter rises. Dero et al. [4] depicted the impacts of Darcy–Forchheimer permeable material on the flow of revolving radiation magnetism over a decreasing hybrid shape. They deduced that the thermal flow ratio decreases with the maximum value of copper volume concentration. Srinivasacharya and Surender [5] analyzed the impacts of double stratification on the free forced convective boundary flow of viscous fluid particles across a vertical surface in permeable material. They discovered that the ratio of temperature and energy decreases significantly for higher Darcy parameter. Ayodeji et al. [6] developed flow separation impacts of mass particles of slip flow on fluid particles passing through a permeable stretched material. They discovered that surface tension rises as the slip velocity increases and the mass slip falls. Khan and Pop [7] performed a tubular analysis on a

laminar nanofluid problem form a stretching geometry. They observed that the Sherwood number is reduced by increasing the Prandtl number. Ghalambaz et al. [8] determined the physical flow of nanoparticles across a porous stretched material. James et al. [9] developed a dynamic thickness of fluid particles through a conductive cylinder inserted in a porous material with heat energy. They observed that the Nusselt and Sherwood numbers increase along the stretching surface due to maximum value of thermal radiation parameter. The researcher [10] analyzed the effects of baffles on nanofluid-filled enclosures used in convective heat transfer. Entropy analysis on circular pseudo-plastic flow with MHD utilizing the Keller box approach is carried out numerically in [11]. The researcher [12] performed a numerical analysis of the effects of Reynolds on micro-polar flow in a channel.

Nanofoam technology, nano-emulsion technology, and injected fluids are very important during the EOR process. The mechanism of nanofluid EOR is based on the nanoparticle adsorption effect. Nanoparticles can be adsorbed on mineral surfaces and thus alter the wettability of minerals from oil-wet to water-wet conditions. Nanoparticles can also be adsorbed on the oil/water surface, which alters the oil/water interfacial tension, resulting in the formation of emulsions. For the improvement of vehicle aerodynamics, there is a higher demand for braking systems with higher and more efficient heat dissipation mechanisms and properties to reduce drag forces. To overcome this situation, nanofluids are very important to reduce friction and maximum heat transfer performance. Rana and Bhargava [13] illustrated the mechanism of laminar fluid of nanoparticles across a quasi-stretched surface by using finite element method. Irfan et al. [14] constructed the MHD nano-liquid flow across a dynamic surface area by using numerical methods with different liquid properties. Ferdows et al. [15] studied the free forced convective boundary flow of nanofluid particles across the porous material by using stretched shape. Gorla and Sidawi [16] explored the heat transfer assessment of free convective flow along the stretching sheet in the presence of suction and blowing effects. Wang [17] studied the thermal boundary layer performance of free convective fluid across the stretching sheet numerically. Sandeep et al. [18] computed the MHD nanofluid particles in an irregular boundary layer past a stretching surface with variable intrinsic heat generation. Khan and Pop [19] performed the formulation of a stretching sheet in porous material filled by base fluid. Alam et al. [20] analyzed the nanofluid particles across a quasi-stretched and permeable shape. Uddin et al. [21] developed a free forced convective nanofluid problem though a thermally conductive stretched surface immersed in a porous material filled with nanofluid. Jafar et al. [22] illustrated the MHD convective problem of nanofluid particles in a porous material across a stretched surface. Prasannakumara et al. [23] performed the impact of particles' dispersion on nanofluid flow with thermal convection through a stretched surface immersed in porous material. Narender et al. [24] elaborated the chemical process and viscoelastic dispersion in a numerical solution of mixed convective nanofluid flow along a stretching sheet. Dessieand Fissha [25] studied free forced convective flow of Maxwell nano fluid particles across a horizontal porous surface. Gireesha et al. [26] studied a numerical simulation for fluid particle suspension and MHD flow for heat transmission across a stretch sheet contained in a quasi-permeable medium. They observed that the size of the atmospheric boundary layer is decreased by floating small dust particles in pure solution. Lakshmi et al. [27] investigated the solution of mass transfer of multiple particles produced by a continuously stretched surface by using Runge Kutta Fehlberg RKF (Runge Kutta Fehlberg is a numerical tool to convert nonlinear ordinary differential equations into system of algebraic equations) simulation. They concluded that with rising nanoparticle concentration, the size of the energy, temperature, and chemical boundary regions reduces.

Higher temperature at the tool–work interface causes failure of the cutting tools and the formation of micro cracks. The reason behind the high temperature formation is the high rate of friction between tool–work and tool–chip interfaces caused by the continuous rubbing action of forming the chip with the tool face and the shearing failure of chip. To overcome this problem, the solution which is most widely used comes into picture; that is, implementation of nanofluid. The purpose of nanofluid such as cutting fluids is to

provide cooling and to reduce the friction between the tool and work piece at the shear zone. It is well known that the application of minimum quantity lubrication (MQL) as a nanofluid is more preferable than other fluids for the cooling technique. To increase the effectiveness of MQL, the addition of nanoparticles is very important. Minimum quantity lubrication fulfills the desire of almost all the machining processes where the cooling and lubrication is a must. The machining processes in which MQL has wide application are turning, grinding, drilling, and milling. On account of emerging 'nanotechnology', the concept of nanofluid lubrication has been developed. Nano lubrication is a process of effectively cooling and lubricating cutting zone during any machining process by involving nanofluid instead of the normally used fluids. Krishnaan and Chamkha [28] analyzed the impacts of Maxwell and ion drift on mixed convective mechanism of nanofluid flow particles across a stretched surface enclosed in a permeable medium. Gireesha et al. [29] illustrated the viscoelastic fluid flow separation past a stretching sheet filled with nanoparticles. They found that the temperature increased with a higher Prandtl number and the volumetric percentage of micro-particles. The viscous dissipative, magnetohydrodynamics, and radiations impacts on laminar fluid flow along the stretching geometry were examined by Maranna et al. [30]. For various engineering applications, Mabood et al. [31] carried out magnetohydrodynamics and entropy analysis for the Jeffrey nanofluid phenomenon across the stretching surface. The nonlinear boundary value problems modeling steady polymer flows in domains with impermeable solid walls were studied by Baranovskii [32]. Following these authors, many people believe that nanotechnology is the most important factor for the next large industrial revolution of this century. The nanofluid particles have great capacity to manipulate matter's molecular structure in order to innovate in almost every sector of the economy and in government-run projects, including national security, transportation, the environment, medical and physical sciences, and electronic cooling.

The goal of present paper is to reduce friction and heat generation between tool–chip and tool–work in the machining process cutting zone by using nanofluids. Thus, in this paper, we investigate the simultaneous effects of temperature-dependent density and thermophoresis on the flow of nanofluid over a stretching porous surface. In particular, the variations of Brownian motion and thermophoresis are analyzed. All the above-mentioned studies are found to deal with a small temperature difference between the surface and ambient fluid. However, circumstances arise where this temperature difference is high. In this situation, the Boussinesq approximation becomes inappropriate (see Kakac and Yenar [33]). That is why, for the particular situation where a high temperature difference arises, the density is assumed as a function of temperature. The effects of variable density on heat–mass transfer and the nanoparticle fraction phenomenon of nanofluid across a stretching sheet placed in porous material with thermophoresis and Brownian motion effects have been investigated numerically, building on the concepts of previous research [7]. The non-similar expressions are numerically integrated with the Keller Box method. The numerical outcomes are deduced in graphs and tabular form with the help of the MATLAB program. The physical characteristics of unknown variables in the flow model, such as velocity graph, temperature field graph, concentration graph, skin friction rate, rate of heat transfer, and rate of mass transfer, have been plotted. The findings of this research, to the best of our knowledge, are original and have never been published.

2. The Flow Geometry and Mathematical Formulation

The current mechanism is computed for numerical outcomes of the variable density impact on heat–mass transfer and the nanoparticle fraction phenomenon of nanofluid across a stretching sheet in a porous material with thermophoresis and Brownian motion effects. Using stream function forms, the extended issue will be reduced to a set of partial differential conditions, which will subsequently be converted into ordinary conditions. By incorporating the Keller Box approach with the finite difference FDM method (finite difference method is a numerical tool to convert nonlinear ordinary differential equations into system of algebraic equations), the molding issue will be solved. Graphical and

tabular interpretations of the simulation solution for the material properties under analysis will be used.

Think about the incompressible, steady nanofluid in two dimensions by observing Figure 1; u and v are the velocity fields in the x and y orders, respectively, where x and y are parallel and perpendicular to the stretching porous sheet; temperature is denoted by T; free stream temperature is denoted by T_∞; fluid thermal conductivity is denoted by κ; and specific heat is denoted by C_p. Fluid density is represented with ρ; the density of particles is denoted by ρ_p; the kinematic fluid viscosity is denoted by $\nu = \mu/\rho$, the fluid density is denoted by ρ_f; and the gravitational acceleration is denoted by g. The governing equations for the current physical model are given below:

$$\frac{\partial(\rho u)}{\partial x} + \frac{\partial(\rho v)}{\partial y} = 0, \tag{1}$$

$$\rho\left(u\frac{\partial u}{\partial x} + v\frac{\partial u}{\partial y}\right) = -\frac{\partial p}{\partial x} + \mu\left(\frac{\partial^2 u}{\partial x^2} + \frac{\partial^2 u}{\partial y^2}\right) - \frac{\in^2 \mu}{k}u + g(\rho_\infty - \rho), \tag{2}$$

$$\rho\left(u\frac{\partial v}{\partial x} + v\frac{\partial v}{\partial y}\right) = -\frac{\partial p}{\partial y} + \mu\left(\frac{\partial^2 v}{\partial x^2} + \frac{\partial^2 v}{\partial y^2}\right) - \frac{\in^2 \mu}{k}v + g(\rho_\infty - \rho), \tag{3}$$

$$(\rho c_p)_f\left(u\frac{\partial T}{\partial x} + v\frac{\partial T}{\partial y}\right) = \kappa\left(\frac{\partial^2 T}{\partial x^2} + \frac{\partial^2 T}{\partial y^2}\right) + (\rho c_p)_p\left\{D_B\left(\frac{\partial C}{\partial x}\frac{\partial T}{\partial x} + \frac{\partial C}{\partial y}\frac{\partial T}{\partial y}\right) + \left(\frac{D_T}{T_\infty}\right)\left[\left(\frac{\partial T}{\partial x}\right)^2 + \left(\frac{\partial T}{\partial y}\right)^2\right]\right\}, \tag{4}$$

$$u\frac{\partial C}{\partial x} + v\frac{\partial C}{\partial y} = D_B\left(\frac{\partial^2 C}{\partial x^2} + \frac{\partial^2 T}{\partial y^2}\right) + \left(\frac{D_T}{T_\infty}\right)\left(\frac{\partial^2 T}{\partial x^2} + \frac{\partial^2 T}{\partial y^2}\right). \tag{5}$$

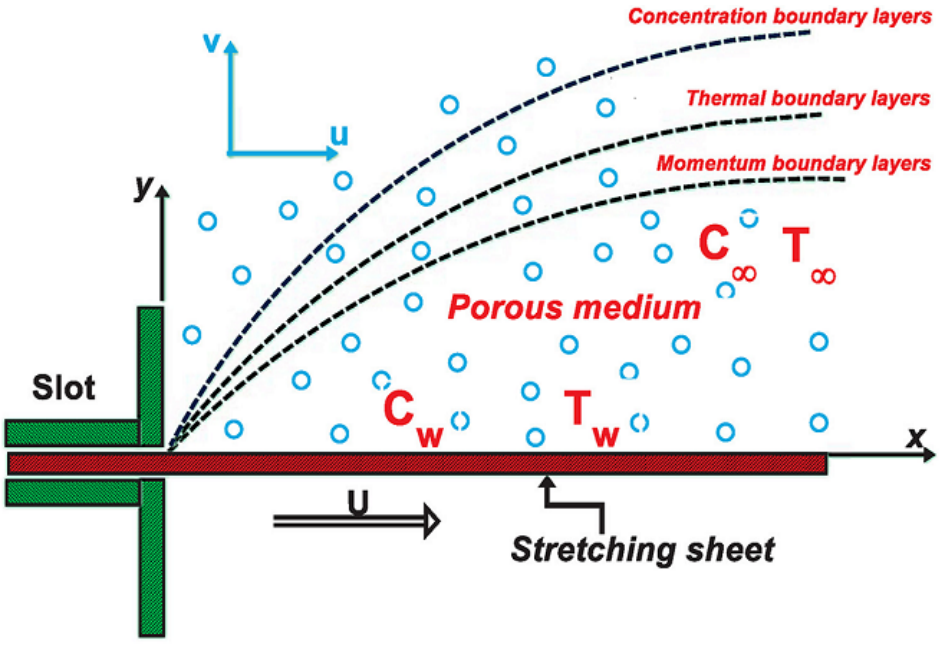

Figure 1. Coordinate system and flow geometry.

The boundary conditions of the present model are

$$v = 0, \quad u = u_w(x) = ax, \quad T = T_w, \quad C = C_w \text{ at } y = 0, \tag{6}$$

$$u \to 0\,, \quad T \to T_\infty\,, \quad C \to C_\infty \quad \text{as} \quad y \to \infty.$$

The preceding description outlines the appropriate boundary conditions for the temperature and velocity components. P represents fluid pressure, ρ represents the density of the base fluid, α represents thermal diffusivity, ν represents kinematic viscosity, a represents a positive constant, and D_B represents the Brownian diffusion coefficient, D_T represents the thermophoretic diffusion coefficient, and $\tau = (\rho c)p/(\rho c)f$ represents the fluid heat capacity and the nanoparticle materials heat capacity ratio, where ρ represents density and c represents the coefficient of volume expansion.

3. Stream Functions and Similarity Variables

The appropriate unitless stream functions ψ and similarity variables to transform PDEs into ODEs are given in Equations (7) and (8) with η and dimensionless temperature θ:

$$u = \frac{1}{\overline{\rho}}\frac{\partial \psi}{\partial y}, \qquad v = -\frac{1}{\overline{\rho}}\frac{\partial \psi}{\partial x}, \qquad \phi(\eta) = \frac{C - C_\infty}{C_w - C_\infty} \qquad p = p_o(constant), \tag{7}$$

$$\psi = (av)^{\frac{1}{2}} x f(\eta), \qquad \theta(\eta) = \frac{T - T_\infty}{T_w - T_\infty}, \qquad \eta = (a/v)^{1/2} y. \tag{8}$$

Equations (7) and (8) are used to turn the PDEs from Equations (1)–(6) into nonlinear ODEs;

$$\left(f'^2 - ff''\right) = e^{-n\theta}\left(f''' - n\theta' f''\right) - e^{n\theta}\Omega f' - \lambda\left(\frac{1 - e^{n\theta}}{1 - e^{-n}}\right), \tag{9}$$

$$\frac{e^{-n\theta}}{p_r}(\theta'' - n\theta'^2) + f\theta' + \left(e^{-n\theta}\right)^2\left[N_B\phi'\theta' + N_T\theta'^2\right] = 0, \tag{10}$$

$$\left(e^{-n\theta}\right)^2[(\phi'' - n\phi'\theta') + \frac{N_T}{N_B}(\theta'' - n\theta'^2)] + Lef\phi' = 0, \tag{11}$$

where $Pr = \frac{\nu}{\alpha}$ is Prandtl parameter, $Le = \frac{v}{D_B}$ is Lewis parameter, $N_B = \frac{(\rho c)_p D_B(\phi_w - \phi_\infty)}{(\rho c)_f v}$ is a Brownian motion number, $\Omega = \frac{\varepsilon^2 v}{ka}$ is the porous number, dimensionless temperature is denoted by θ, kinematic viscosity is denoted by $\nu = \frac{\mu}{\rho}$, and $N_T = \frac{(\rho c)_p D_T(T_w - T_\infty)}{(\rho c)_f v T_\infty}$ is the thermophoresis parameter. The boundary conditions in (6) then become

$$f(\eta) = 0, \qquad f'(\eta) = 1, \qquad \theta(\eta) = 1, \qquad \phi(\eta) = 1 \text{ at } \eta = 0, \tag{12}$$

$$f'(\infty) = 0, \qquad \theta(\infty) = 0, \qquad \phi(\infty) = 0 \text{ at } \eta \to \infty.$$

4. Computational Scheme and Solution Methodology

The connected mathematical nonlinear PDEs model is changed in a similar ODEs model with similarity variables using an appropriate stream function formulation. In Equations (9)–(11), similar coupled ODE models with given boundary conditions are solved using the iterative Keller Box approach (12). The additional independent quantities are introduced by $p(\eta)$; $q(\eta)$, $u(\eta)$, $v(\eta)$, $l(\eta)$, and $m(\eta)$ by using Equation (13):

$$f' = p', f'' = p' = \mathrm{q}, f''' = q', \varphi' = u, \tag{13}$$

$$\varphi'' = u' = v, \varphi''' = v', \theta' = l, \theta'' = l' = m.$$

To overcome the issues, the Equations (9)–(12) become easier to solve when the straightforward forms are

$$f' = p \Rightarrow f' - p = 0, \tag{14}$$

$$p' = q \Rightarrow p' - q = 0, \tag{15}$$

$$\phi' = u \Rightarrow \phi' - u = 0, \tag{16}$$

$$u' = v \Rightarrow u' - v = 0, \tag{17}$$

$$\theta' = l \Rightarrow \theta' - l = 0, \tag{18}$$

$$\left(p^2 - \mathrm{fq}\right) = e^{-n\theta}\left(q' - nlq\right) - e^{-n\theta}\Omega p - \lambda\left(\frac{1 - e^{n\theta}}{1 - e^{-n}}\right), \tag{19}$$

$$\frac{1}{p_r}\left(m - nl^2\right) + fl + e^{-n\theta}\left[N_B ul + N_T l^2\right] = 0, \tag{20}$$

$$\left(e^{-n\theta}\right)^2\left[(v - nlu) + \frac{N_T}{N_B}\left(m - nl^2\right)\right] + Lefu = 0. \tag{21}$$

The reduced boundary conditions are

$$f(0) = 0, \quad P(0) = 1, \quad \theta(0) = 1, \quad \varphi(0) = 1, \quad at \quad \eta = 0, \tag{22}$$

$$P(\infty) \to 0, \quad \theta(\infty) \to 0, \quad \varphi(\infty) \to 0, \quad as \quad \eta \to \infty.$$

Now consider the midpoint values with segment η_{n-1}, η_n with $\eta_{n-\frac{1}{2}}$ by using Equation (23):

$$\eta_0 = 0, \quad \eta_n = \eta_{n-1} + h_n, \quad \eta_n = \eta_\infty. \tag{23}$$

The above Equations (14)–(22) are transformed, with average and central difference forms given in Equation (24):

$$f' = \frac{f_n - f_{n-1}}{h_n}, \qquad f = \frac{f_n + f_{n-1}}{2} = f_{n-\frac{1}{2}}, \tag{24}$$

and

$$f_n - f_{n-1} - \frac{1}{2}h_n(p_n + p_{n-1}) = 0, \tag{25}$$

$$p_n - p_{n-1} - \frac{1}{2}h_n(q_n + q_{n-1}) = 0, \tag{26}$$

$$\phi_n - \phi_{n-1} - \frac{1}{2}h_n(u_n + u_{n-1}) = 0, \tag{27}$$

$$u_n - u_{n-1} - \frac{1}{2}h_n(v_n + v_{n-1}) = 0, \tag{28}$$

$$\theta_n - \theta_{n-1} - \frac{1}{2}h_n(l_n + l_{n-1}) = 0, \tag{29}$$

$$\frac{1}{4}(p_n + p_{n-1})^2 - \frac{1}{4}(f_n + f_{n-1})(q_n + q_{n-1}) = \frac{1}{2h_n}(2 - n\theta_n + n\theta_{n-1})(q_n - q_{n-1}) - \frac{n}{8}(2 - n\theta_n + n\theta_{n-1})(l_n + l_{n-1})(q_n + q_{n-1}) - \frac{\Omega}{4}(2 - n\theta_n + n\theta_{n-1})(p_n + p_{n-1}) - \frac{\lambda}{2}(\theta_n + \theta_{n-1}), \tag{30}$$

$$\frac{1}{2P_r}(m_n + m_{n-1}) - \frac{n}{4P_r}(l_n + l_{n-1})^2 + \frac{1}{4}(f_n + f_{n-1})(l_n + l_{n-1}) + \frac{N_b}{8}(2 - n\theta_n - n\theta_{n-1})(u_n + u_{n-1})(l_n + l_{n-1}) + \frac{N_t}{8}(2 - n\theta_n - n\theta_{n-1})(l_n + l_{n-1})^2 = 0, \tag{31}$$

$$1 + \frac{n^2}{2}(\theta_n + \theta_{n-1})^2 - n(\theta_n + \theta_{n-1})\left[\frac{1}{2}(v_n + v_{n-1}) - \frac{n}{4}(l_n + l_{n-1})(u_n + u_{n-1})\right]\frac{N_T}{N_b}\left(\frac{1}{2}(m_n + m_{n-1}) - \frac{n}{4}(l_n + l_{n-1})^2\right) + \frac{Lef}{2}(u_n + u_{n-1}) = 0, \tag{32}$$

along with boundary conditions

$$f_0 = 0,\ \phi_0 = 1,\ p_0 = 0,\ \theta_0 = 1,\ u = 1,\ \text{at}\ \eta = 0, \tag{33}$$

$$p_n \to 0,\ \theta_n \to 0,\ \phi_0 \to 0,\ as\eta \to \infty,$$

and now by using the iterative Newton–Raphson method for a smooth algorithm described below:

$$f_n^{k+1} = f_n^k + \delta f_n^k,\ \ p_n^{k+1} = p_n^k + \delta p_n^k, \tag{34}$$

$$q_n^{k+1} = q_n^k + \delta q_n^k,\quad \theta_n^{k+1} = \theta_n^k + \delta\theta_n^k,$$

$$u_n^{k+1} = u_n^k + \delta u_n^k,\quad \phi_n^{k+1} = \phi_n^k + \delta\phi_n^k,$$

$$v_n^{k+1} = v_n^k + \delta v_n^k,\quad l_n^{k+1} = l_n^k + \delta l_n^k.$$

In the same way as in the standard Newton–Raphson approach, equations become simpler by eliminating any instances of powers greater than the first power:

$$\delta f_n - \delta f_{n-1} - \frac{1}{2}h_n(\delta p_n + \delta p_{n-1}) = (r_1)_n, \tag{35}$$

$$\delta p_n - \delta p_{n-1} - \frac{1}{2}h_n(\delta q_n + \delta q_{n-1}) = (r_2)_n, \tag{36}$$

$$\delta\phi_n - \delta\phi_{n-1} - \frac{1}{2}h_n(\delta v_n + \delta v_{n-1}) = (r_3)_n, \tag{37}$$

$$\delta u_n - \delta u_{n-1} - \frac{1}{2}h_n(\delta v_n + \delta v_{n-1}) = (r_4)_n, \tag{38}$$

$$\delta\theta_n - \delta\theta_{n-1} - \frac{1}{2}h_n(\delta l_n + \delta l_{n-1}) = (r_5)_n. \tag{39}$$

The equations are given below in their condensed form, once more utilizing Equations (35)–(39) in Equations (30)–(33):

$$(a_1)_n\delta p_n + (a_2)_n\delta p_{n-1} + (a_3)_n\delta f_n + (a_4)_n\delta f_{n-1} + (a_5)_n\delta q_n + (a_6)_n\delta q_{n-1} + (a_7)_n\delta\theta_n + (a_8)_n\delta\theta_{n-1} + (a_9)_n\delta l_n + (a_6)_n\delta l_{n-1} = (r_6)_n, \tag{40}$$

$$(b_1)_n\delta m_n + (b_2)_n\delta m_{n-1} + (b_3)_n\delta l_n + (b_4)_n\delta l_{n-1} + (b_5)_n\delta\theta_n + (b_6)_n\delta\theta_{n-1} + (b_7)_n\delta u_n + (b_8)_n\delta g_{n-1} + (b_9)_n\delta f_n + (b_{10})_n\delta f_{n-1} = (r_7)_n, \tag{41}$$

$$(c_1)_n\delta\theta_n + (c_2)_n\delta\theta_{n-1} + (c_3)_n\delta v_n + (c_4)_n\delta v_{n-1}(c_5)_n\delta l_n + (c_6)_n\delta l_{n-1} + (c_7)_n\delta f_n + (c_8)_n\delta f_{n-1} + (c_9)_n\delta u_n + (c_{10})_n\delta u_{n-1} = (r_8)_n. \quad (42)$$

Recalling the precise boundary conditions without iteration, we take steps to make sure that these correct values are preserved across all iterations:

$$\delta f_0 = 0, \qquad \delta\phi_0 = 1, \quad \delta p_0 = 1, \qquad \delta\theta_0 = 1 \quad (43)$$

$$\delta p_n = 0, \qquad \delta\theta_n = 0, \qquad \delta\phi_n = 0$$

5. Matrix Form of Vector Equations

The matrix-based structure of the aforementioned difference equations is a crucial next step. If it is conducted incorrectly, the strategy either becomes incredibly ineffective since the matrix has no visible structure, or produces zero solutions due to a solitary matrix with zero determinants or sub-matrices. The matrix form of vector equations is given as

$$A\delta = r \quad (44)$$

$$[A] = \begin{bmatrix} [A_1][C_1] & \cdots & \cdots \\ [B_2][A_2][C_2] & & \\ \vdots & \ddots & \vdots \\ \vdots & \cdots & [B_{n-1}][A_{n-1}][C_{n-1}] \\ & & [B_n][A_n] \end{bmatrix}, \quad [\delta] = \begin{bmatrix} [\delta_1] \\ [\delta_2] \\ \vdots \\ [\delta_{n-1}] \\ [\delta_n] \end{bmatrix}, \quad [r] = \begin{bmatrix} [r_1] \\ [r_2] \\ \vdots \\ [r_{n-1}] \\ [r_n] \end{bmatrix} \quad (45)$$

6. Quantitative and Physical Reasoning

Due to excessive heating, various physical problems are go unaddressed in modern technologies and industries. The current physical phenomena addressed the variable density impact on heat–mass transfer and the nanoparticle fraction phenomenon of nanofluid across stretching sheet placed in porous material with thermophoresis and Brownian motion effects and has been explored numerically. The coupled partial differential equations of the present nanofluid mechanism are changed in nonlinear coupled ordinary differential equations with defined stream functions and similarity variables for smooth algorithm and integration. The changed ODEs are again converted in similar forms for numerical outcomes by applying the Keller Box approach. The numerical outcomes are deduced in graphs and tabular form with the help of the MATLAB program. How physical quantities such as velocity graphs, temperature graphs, and concentration graphs behave together with their slopes, which represent the rates of mass transfer, heat transfer, and skin friction under the influence of various flow model parameters, is examined. The impact of physical parameters, such as Prandtl parameter Pr, temperature density number n, Lewis parameter L_e, thermophoresis parameter Nt, buoyancy number λ, Brownian motion number Nb, and porous number Ω, are drafted in numerical and physical form.

Figure 2a–c shows the impact of the Prandtl number on the velocity graph, the temperature graph and concentration graph, respectively. The Figure 2a shows the physical quantity of the velocity graph for diverse P_r = 0.3, 0.5, 0.7, 1.0. It is deduced that the velocity graph is enhanced for minimum Pr = 0.3 and reduced for higher Pr = 1.0. It is noted that the temperature θ plot is increased for minimum Pr = 0.3 and reduced for higher Pr = 1.0 in Figure 2b. The prominent variation is noted in the temperature plot against Pr. In Figure 2c, the fluid concentration profile is enhanced for minimum Pr = 0.3 and reduced for higher Pr = 1.0. Figure 3a–c illustrates the effect of different values of λ = 1.0, 5.0, 10.0, 15.0 on the velocity U, temperature θ, and concentration ϕ profiles. In Figure 3a, it is seen that velocity U profile is increased at a maximum of λ = 15.0 and reduced for a minimum λ = 1.0, with good response. Figure 3b represents the effect of λ on the $\theta(\eta)$ graph. It can be seen

that the temperature profile is reduced for higher λ = 15.0 but increased by decreasing λ = 1.0. Figure 3c indicates the effect of λ on various values of $\phi(\eta)$ plot. That the concentration profile increased by decreasing λ = 1.0 but decreased by increasing λ = 15.0 is examined in Figure 3c. The prominent variation in every plot is noted for various choices of buoyancy number λ. Figure 4a–c shows the physical plots of velocity U, temperature θ, and concentration ϕ plots for diverse values of $n = 0.0,\ 0.3,\ 0.6,\ 1.0$. In Figure 4a, it is noted that the velocity U plot is enhanced for minimum $n = 0.0$ and reduced for maximum $n = 1.0$. Figure 4b illustrated the temperature profile along η. It is deduced that the $\theta(\eta)$ of fluid is decreased with the increase of n. Figure 4c displays the impact of density n on the concentration graph, which is decreased by increasing $n = 1.0$, but increased by decreasing $n = 0.0$. The prominent variation in every graph is noted for various choices of density n. Figure 5a–c presented the physical outcomes of velocity U, temperature θ, and $\phi(\eta)$ plots for $\Omega = 0.5,\ 1.5,\ 2.0,\ 2.5$. It is noted that the velocity profile is enhanced for minimum $\Omega = 0.5$ and reduced for higher $\Omega = 2.5$ by keeping other parameters fixed, as in Figure 5a. The temperature θ graph is enhanced for maximum $\Omega = 2.5$ and the other value of Ω the $f'(\eta)$ plot is similar in Figure 5b. The concentration ϕ plot is enhanced by increasing $\Omega = 2.5$ but decreased by decreasing $\Omega = 0.5$ in Figure 5c. The prominent variation in every plot is noted for various porous number Ω. Figure 6a–c demonstrates the plots of velocity U field, temperature θ field, and concentration ϕ field for diverse values of the thermophoresis parameter N_t by keeping other parameters fixed. The velocity plot is enhanced for maximum N_t = 3.0 and reduced for minimum N_t = 0.1 with good response in Figure 6a. The $\theta(\eta)$ plot is enhanced for maximum $Nt = 3.0$ and reduced for minimum N_t = 0.1 in Figure 6b. The concentration ϕ profile is enhanced by decreasing $Nt = 0.1$ but decreased by increasing N_t = 3.0 in Figure 6c. The prominent variation in every plot is noted for various choices of the thermophoresis parameter N_t. Figure 7a–c depicted the graphs of velocity U, temperature θ , and concentration ϕ graphs for diverse choices of Brownian motion parameter N_b = 0.1, 1.0, 2.0, 3.0, and 4.0 with some other constant parameters. The velocity U plot in increased for higher N_b = 4.0 and decreased at minimum value of N_b = 0.1 by keeping other parameters fixed, as in Figure 7a. The temperature distribution is increased at the maximum value of N_b = 4.0 and reduced for the minimum N_b = 0.1, as in Figure 7b. The concentration ϕ profile is enhanced by decreasing N_b = 0.1 but decreased by increasing N_b = 4.0 in Figure 7c.

From Table 1, it can be seen that skin friction $f''(0)$ is enhanced for large n = 1.0 and the minimum skin friction $f''(0)$ is deduced for small n = 0.0 under the influence of buoyancy parameter λ = 1.5. The heat rate $-\theta'(0)$ is enhanced for larger n = 1.0 and the minimum heat transfer is computed for the smaller n = 0.0, with buoyancy parameter λ = 1.5. The mass transfer is maximum for larger n = 1.0 and the minimum mass transfer is noticed for the smaller $n = 0.0$ with buoyancy parameter λ = 1.5. Table 2 indicated the impact of the Ω parameter for some choices of Ω = 0.5, 1.5, 2.0, and 3.5 past a porous stretching sheet for the physical characteristics of $f''(0), -\phi'(0)$, and $-\theta'(0)$ past the stretching surface with some constant λ = 1.7, M = 3.5, and δ = 1.3. The $f''(0)$ is enhanced for lower Ω = 0.5 while the minimum value of skin friction is examined for the maximum $\Omega = 2.5$. It is mentioned that $-\theta'(0)$ is increased by decreasing $\Omega = 0.5$ and reduced by increasing $\Omega = 2.5$. It can be seen that the mass transfer is raised for the lower choice of $\Omega = 0.5$, while the lowest value of mass transfer is examined for the larger value of $\Omega = 2.5$. Table 3 presents the comparison of heat transfer $-\theta'(0)$ with Gorla and Sidawi [16], Wang [17], and Khan and Pop [18] by reducing Nt and Nb effects for seven values of the Prandtl number—Pr = 0.07, 0.20, 0.70, 2.0, 7.0, 20.0, 70.0—in the presence of the temperature density impact past the stretching porous sheet. It is deduced that the prominent heat transfer is obtained with temperature-dependent density effects for each Pr. Therefore, the current heat transfer results are commensurate with the previous results.

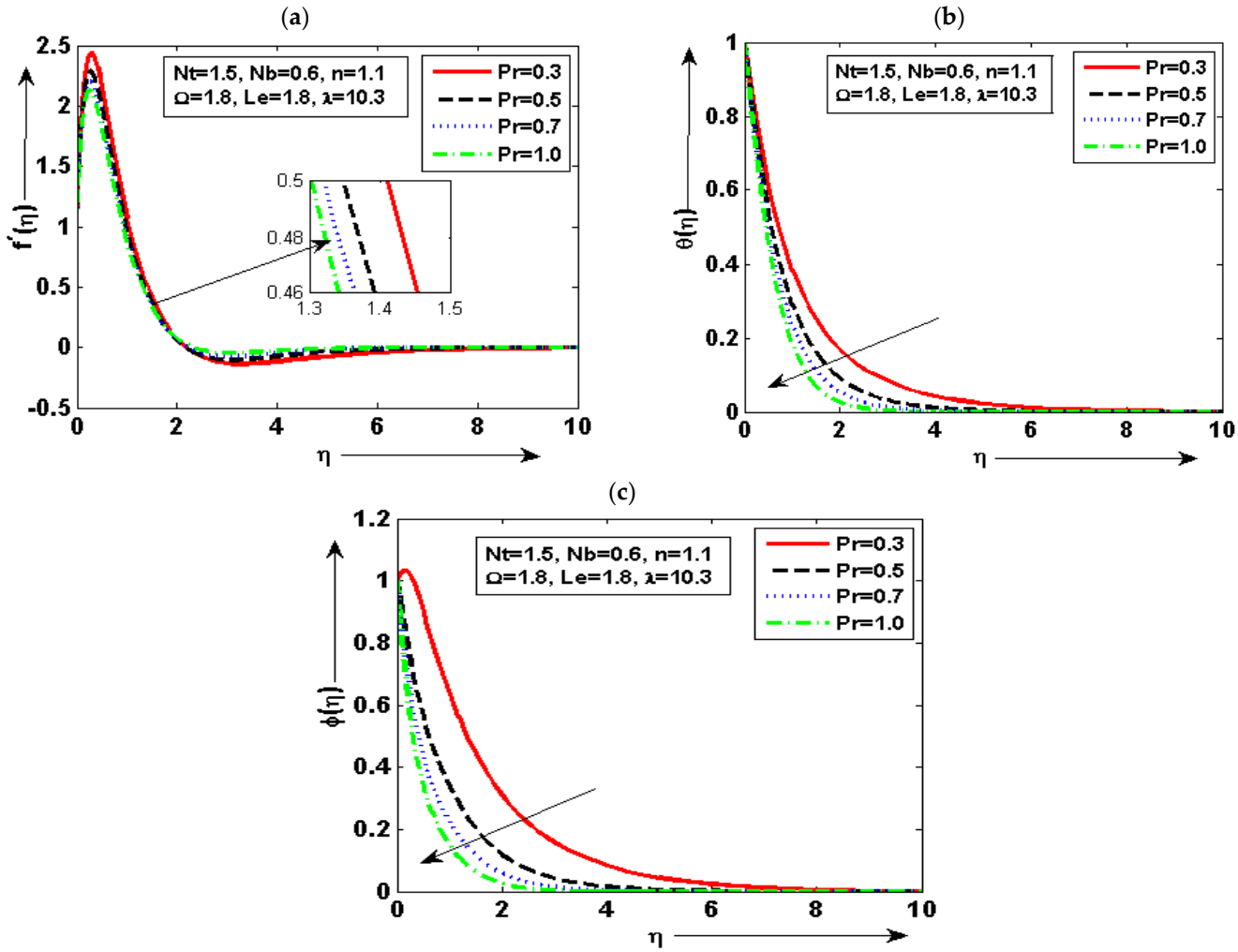

Figure 2. (**a**–**c**) Graphical plots of velocity $f'(\eta)$, temperature θ, and concentration ϕ for some choices of Pr.

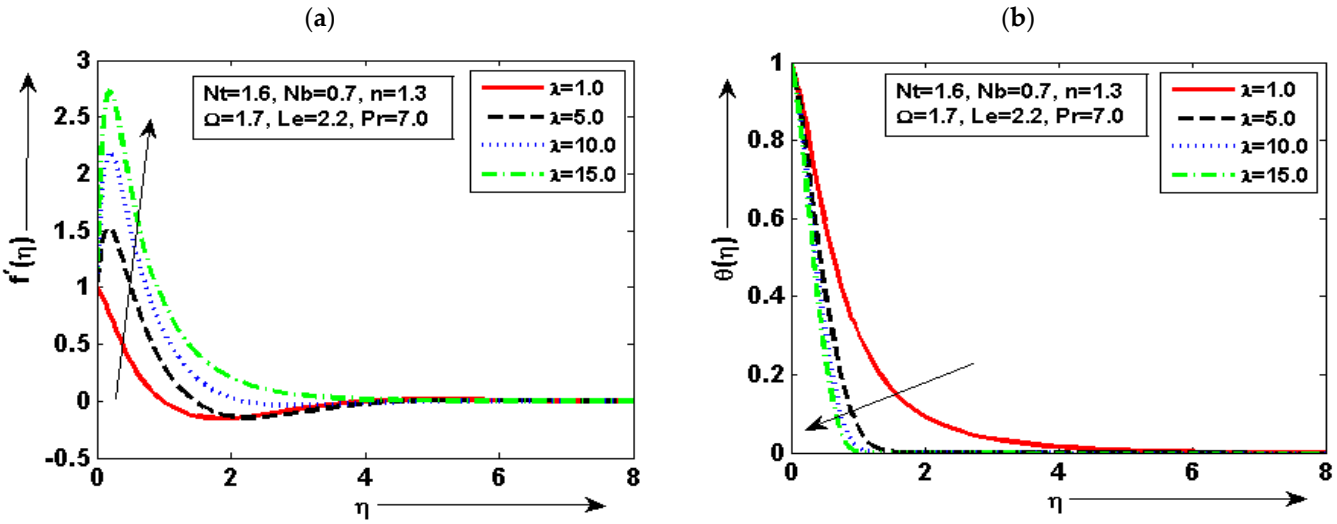

Figure 3. *Cont.*

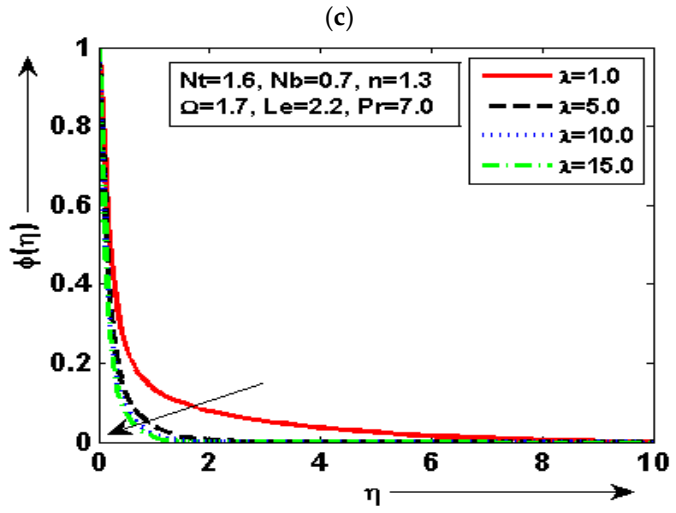

Figure 3. (**a**–**c**) Graphical plots of velocity $f'(\eta)$, temperature θ, and concentration ϕ for some choices of λ.

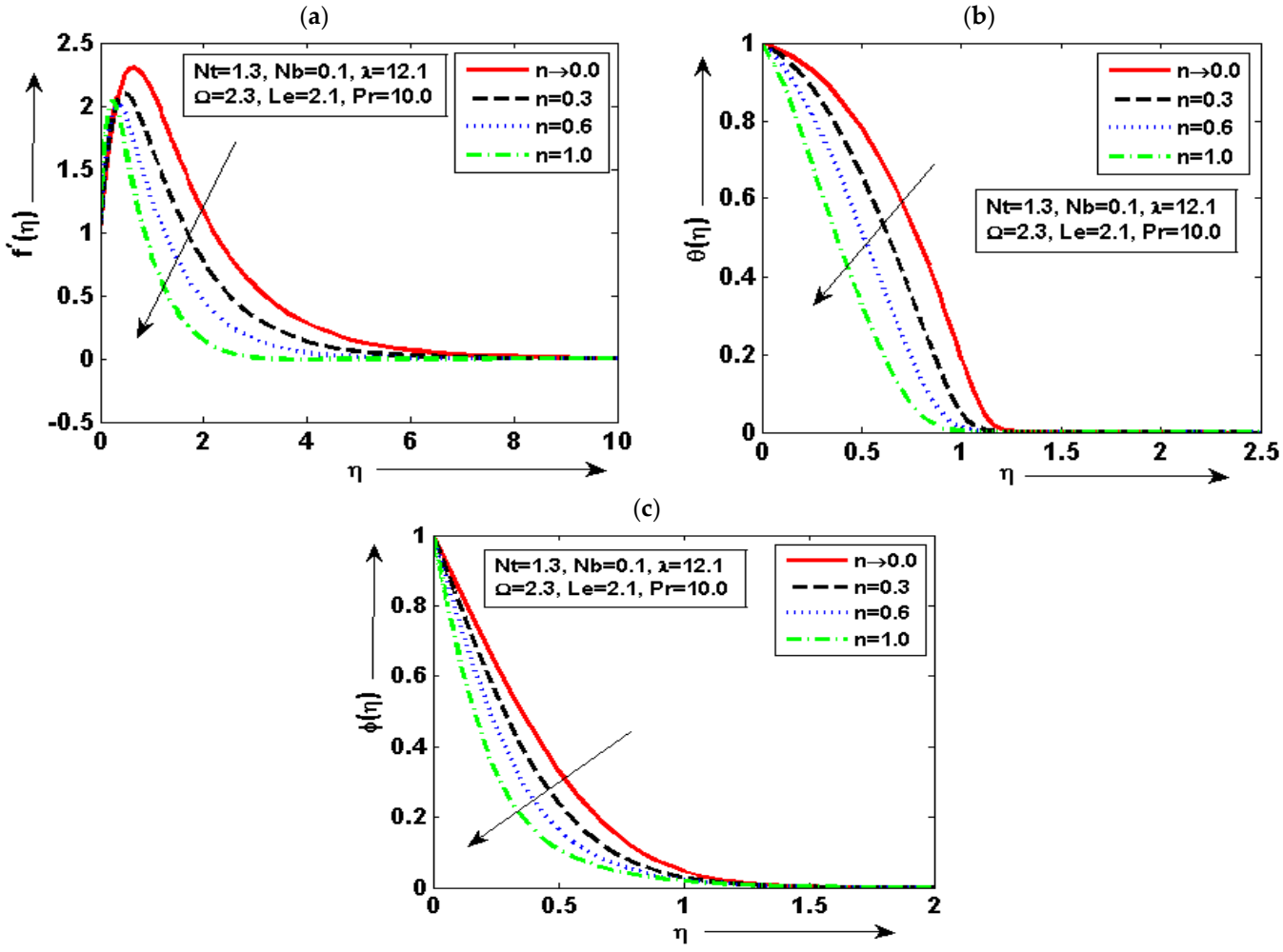

Figure 4. (**a**–**c**) Graphical plots of velocity $f'(\eta)$, temperature θ, and concentration ϕ for some choices of n.

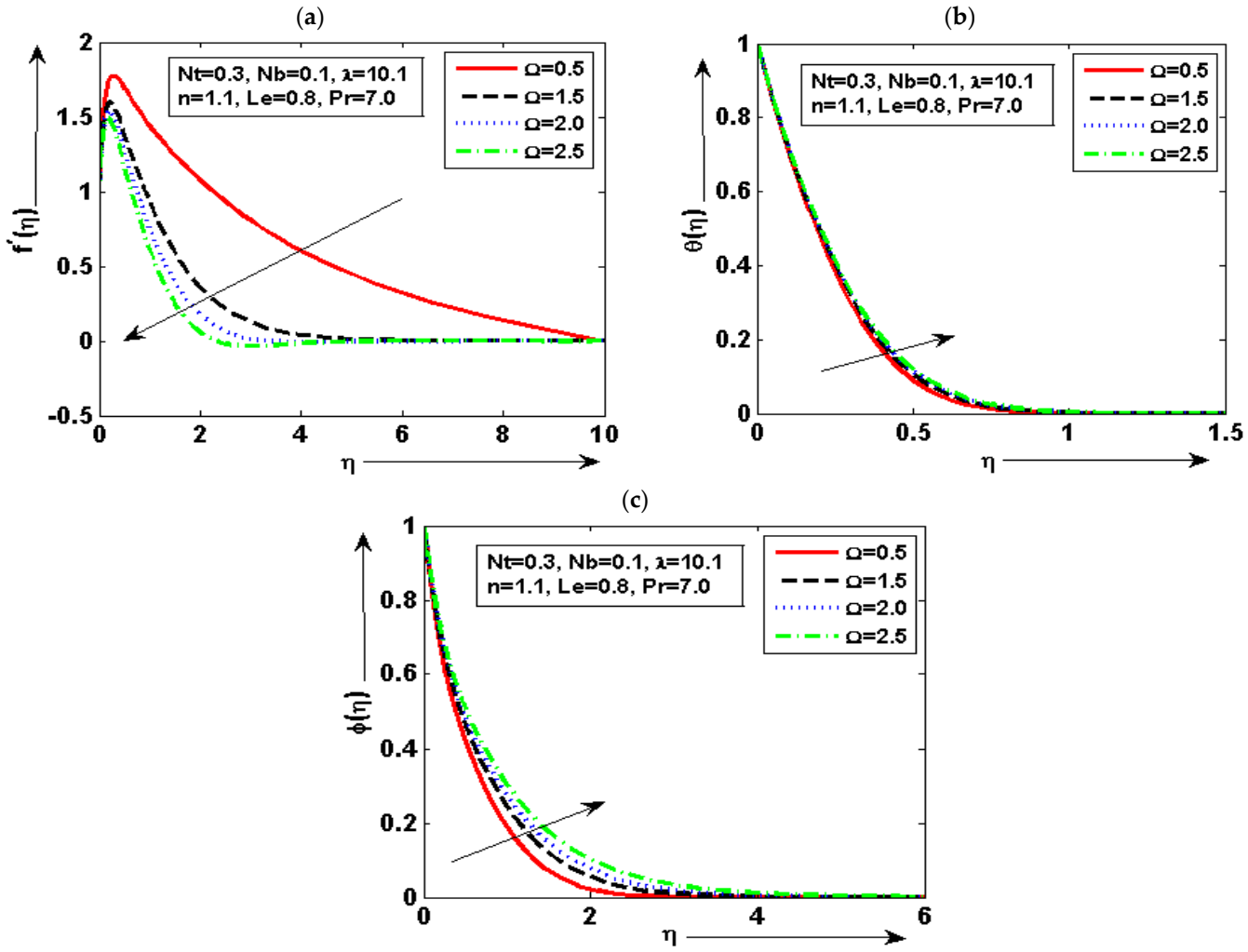

Figure 5. (**a**–**c**) Graphical plots of velocity $f'(\eta)$, temperature θ, and concentration ϕ for some choices of Ω.

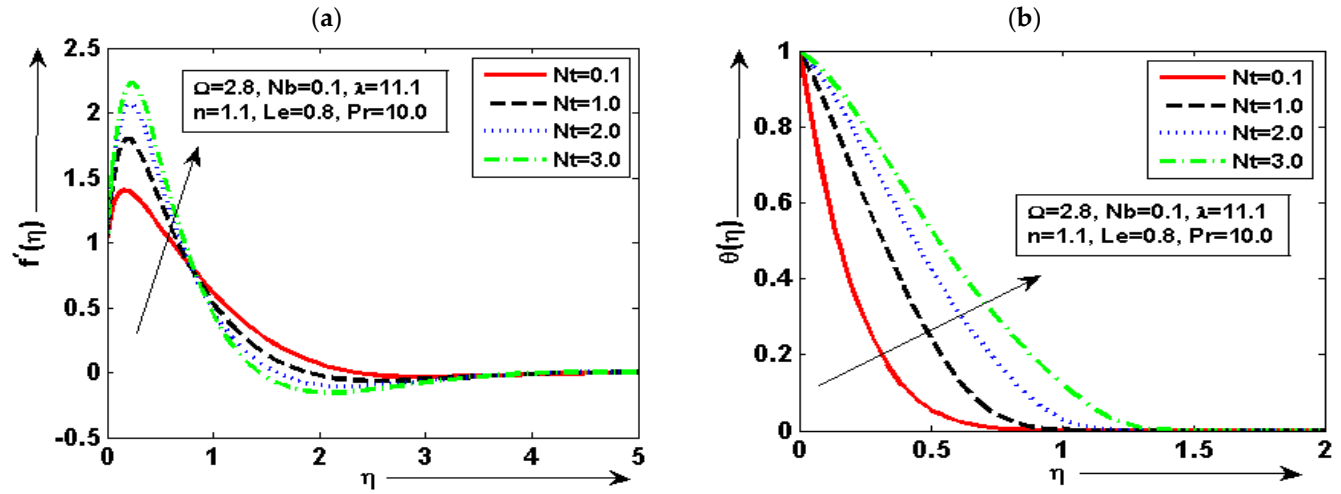

Figure 6. *Cont.*

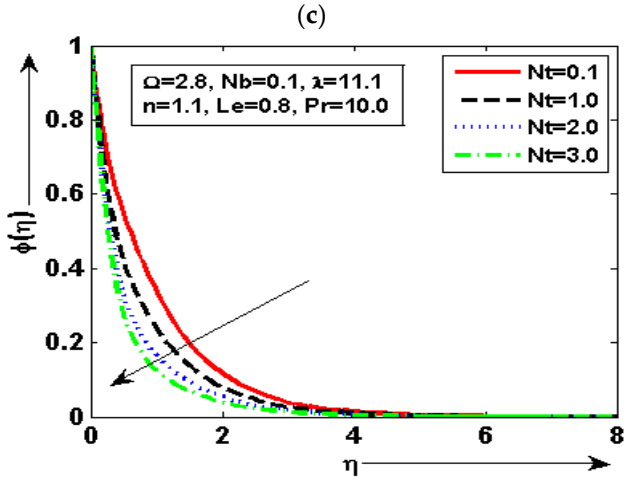

Figure 6. (**a**–**c**) Graphical plots of velocity $f'(\eta)$, temperature θ, and concentration ϕ for some choices of Nt.

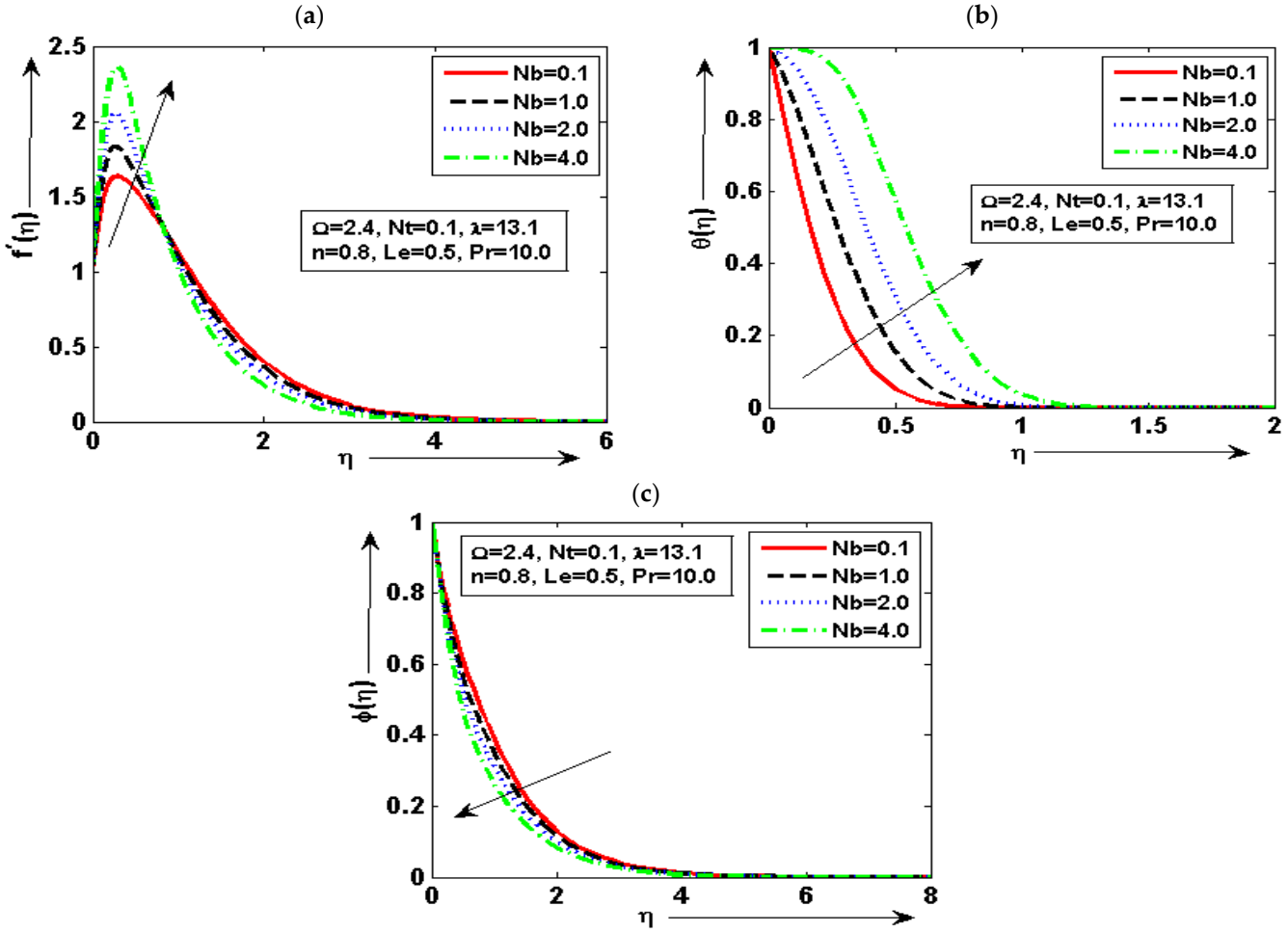

Figure 7. (**a**–**c**) Graphical plots of velocity $f'(\eta)$, temperature θ, and concentration ϕ for some choices of *Nb*.

Table 1. The numerical results for $f''(0)$, $-\theta'(0)$, and for $-\phi'(0)$ for various values of $n = 0.0, 0.3, 0.6, 1.0$ with some parameters fixed.

n=	$f''(0)$	$-\theta'(0)$	$-\phi'(0)$
0.0	4.879240614576633	0.174622809744148	1.514028648228383
0.3	5.553517239574258	0.282093810281554	1.929879513656921
0.6	7.128708418082393	0.451526060701176	2.503545641529655
1.0	11.14056359516007	0.828854931906472	3.609754807395438

Table 2. The numerical outcomes of $f''(0)$, $-\theta'(0)$, and $-\phi'(0)$ with some choices of $\Omega = 0.5, 1.5, 2.5, 3.5$.

Ω	$f''(0)$	$-\theta'(0)$	$-\phi'(0)$
0.5	9.540455671088386	3.024123755289357	2.291019891109566
1.5	8.487572033095056	2.944285424442383	2.085276681324071
2.0	8.086105381985982	2.913421437893619	1.987179978853624
3.5	7.737145446285837	2.886620197701986	1.890161615731341

Table 3. Comparison of numerical results for $-\theta'(0)$ heat transfer for various values of $Pr = 0.07, 0.20, 0.70, 2.0, 7.0, 20.0, 70.0$ with temperature density effects past the stretching porous sheet.

Pr	Gorla and Sidawi [16]	Wang [17]	Khan and Pop [7]	Present Analysis
0.07	0.0656	0.0656	0.0663	0.0688
0.20	0.1691	0.1691	0.1691	0.1696
0.70	0.5349	0.4539	0.4534	0.4616
2.0	0.9114	0.9114	0.9113	0.9632
7.0	1.8905	1.8954	1.8954	1.9064
20.0	3.3539	3.3539	3.3539	3.3905
70.0	6.4622	6.4622	6.4621	6.4962

7. Conclusions

In the present paper, the variable density impact on heat–mass transfer and nanoparticle fraction phenomena of nanofluid across a stretching sheet in porous material with thermophoresis and Brownian motion effects has been explored numerically. The coupled partial differential equations of the present nanofluid mechanism are changed in nonlinear coupled ordinary differential equations with defined stream functions and similarity variables for a smooth algorithm and integration. The changed ODEs are again converted to similar forms for numerical outcomes by applying the Keller Box approach. The numerical outcomes are deduced in graphs and tabular form with the help of the MATLAB program. How physical quantities such as velocity graphs, temperature graphs, and concentration graphs behave together with their slopes, which represent the rates of mass transfer, heat transfer, and skin friction under the influence of various flow model parameters, is examined. The effects of physical variables, such as Prandtl parameter Pr, temperature density number n, Lewis parameter L_e, thermophoresis parameter Nt, buoyancy number λ, Brownian motion number Nb, and porous number Ω, are drafted quantitatively and graphically. The concluding remarks are given as follows:

- The velocity plot is enhanced for minimum quantity of $\mathrm{Pr} = 0.3$ and reduced for maximum $\mathrm{Pr} = 1.0$. The fluid concentration plot is increased for minimum quantity of $\mathrm{Pr} = 0.3$ and reduced for maximum $\mathrm{Pr} = 1.0$;

- The temperature θ graph is at a minimum by higher $\lambda = 15.0$ but increased by decreasing $\lambda = 1.0$. It is deduced that $\theta(\eta)$ of fluid is decreased with the increase of n. The prominent variation in every plot is noted for diverse choices of density number n;
- It is noted that the velocity graph is maximum for the small quantity of $\Omega = 0.5$ and reduced for the larger $\Omega = 2.5$ by keeping the other parameters fixed. It can be seen that the temperature θ plot is enhanced for the maximum choice of $N_b = 4.0$ and reduced for the minimum choice of $N_b = 0.1$;
- The concentration graph is enhanced by decreasing $N_b = 0.1$ but decreased by increasing $N_b = 4.0$. The skin friction $f''(0)$ is increased by increasing the value $n = 1.0$ but decreased by decreasing the value of $n = 0.0$;
- It is found that heat transfer $-\theta'(0)$ is enhanced for the maximum choice of $n = 1.0$ and the minimum choice at lower value of $n = 0.0$. It is also noted that mass transfer is enhanced due to increasing $n = 1.0$ but reduced due to decreasing $n = 0.0$.

Author Contributions: Conceptualization, Z.U.; methodology, Z.U.; software, Z.U.; validation, Z.U.; formal analysis, Z.U.; investigation, Z.U.; resources, Z.U.; data curation, Z.U.; writing—original draft preparation, Z.U.; writing—review and editing, M.S.A.; visualization, M.S.A.; supervision, M.S.A.; project administration, M.S.A.; funding acquisition, M.S.A. All authors have read and agreed to the published version of the manuscript.

Funding: This research received no external funding.

Data Availability Statement: No data is available.

Conflicts of Interest: The authors declare no conflict of interest.

References

1. Pourrajab, R.; Noghrehabadi, A. Bioconvection of nanofluid past stretching sheet in a porous medium in presence of gyrotactic microorganisms with newtonian heating. In *MATEC Web of Conferences*; EDP Sciences: Les Ulis, France, 2018; Volume 220, p. 01004.
2. Sarkar, S.; Endalew, M.F. Effects of melting process on the hydromagnetic wedge flow of a Casson nanofluid in a porous medium. *Bound. Value Probl.* **2019**, *2019*, 43. [CrossRef]
3. Kalavathamma, B.; Lakshmi, C. Effect of variable properties on heat and mass transfer flow of nanofluid over a vertical cone saturated by porous medium under enhanced boundary conditions. *Int. J. Appl. Eng. Res.* **2018**, *13*, 15611–15621.
4. Dero, S.; Shaikh, H.; Talpur, G.H.; Khan, I.; Alharbim, S.O.; Andualem, M. Influence of a Darcy-Forchheimer porous medium on the flow of a radiative magnetized rotating hybrid nanofluid over a shrinking surface. *Sci. Rep.* **2021**, *11*, 24257. [CrossRef]
5. Srinivasacharya, D.; Surender, O. Effect of double stratification on mixed convection boundary layer flow of a nanofluid past a vertical plate in a porous medium. *Appl. Nanosci.* **2015**, *5*, 29–38. [CrossRef]
6. Ayodeji, F.; Abubakar, A.A.; Joy-Felicia, O.O. Effect of Mass and Partial Slip on Boundary Layer Flow of a Nanofluid over a Porous Plate Embedded In a Porous Medium. *IOSR J. Mech. Civ. Eng.* **2016**, *13*, 42–49. [CrossRef]
7. Khan, W.A.; Pop, I. Boundary-layer flow of a nanofluid past a stretching sheet. *Int. J. Heat Mass Transf.* **2010**, *53*, 2477–2483. [CrossRef]
8. Ghalambaz, M.; Noghrehabadi, A.; Ghanbarzadeh, A. Natural convection of nanofluids over a convectively heated vertical plate embedded in a porous medium. *Braz. J. Chem. Eng.* **2014**, *31*, 413–427. [CrossRef]
9. James, M.; Mureithi, E.W.; Kuznetsov, D. Effects of variable viscosity of nanofluid flow over a permeable wedge embedded in saturated porous medium with chemical reaction and thermal radiation. *Int. J. Adv. Appl. Math. Mech.* **2015**, *2*, 101–118.
10. Al-Farhany, K.; Al-Muhja, B.; Loganathan, K.; Periyasamy, U.; Ali, F.; Sarris, I.E. Analysis of Convection Phenomenon in Enclosure Utilizing Nanofluids with Baffle Effects. *Energies* **2022**, *15*, 6615. [CrossRef]
11. Al-Mdallal, Q.; Prasad, V.R.; Basha, H.T.; Sarris, I.; Akkurt, N. Keller box simulation of magnetic pseudoplastic nano-polymer coating flow over a circular cylinder with entropy optimisation. *Comput. Math. Appl.* **2022**, *118*, 132–158. [CrossRef]
12. Sofiadis, G.; Sarris, I. Reynolds number effect of the turbulent micropolar channel flow. *Phys. Fluids* **2022**, *34*, 075126. [CrossRef]
13. Rana, P.; Bhargava, R. Flow and heat transfer of a nanofluid over a nonlinearly stretching sheet: A numerical study. *Commun. Nonlinear Sci. Numer. Simul.* **2012**, *17*, 212–226. [CrossRef]
14. Irfan, M.; Farooq, M.A.; Iqra, T. A new computational technique design for EMHD nanofluid flow over a variable thickness surface with variable liquid characteristics. *Front. Phys.* **2020**, *8*, 66. [CrossRef]
15. Ferdows, M.; Khan, M.; Alam, M.; Sun, S. MHD mixed convective boundary layer flow of a nanofluid through a porous medium due to an exponentially stretching sheet. *Math. Probl. Eng.* **2012**, *2012*, 408528. [CrossRef]
16. Reddy Gorla, R.S.; Sidawi, I. Free convection on a vertical stretching surface with suction and blowing. *Appl. Sci. Res.* **1994**, *52*, 247–257. [CrossRef]

17. Wang, C.Y. Free convection on a vertical stretching surface. *J. Appl. Math. Mech.* **1989**, *69*, 418–420. [CrossRef]
18. Sandeep, N.; Sulochana, C.; Raju, K.; Babu, M.J.; Sugunamma, V. Unsteady boundary layer flow of thermophoretic MHD nanofluid past a stretching sheet with space and time dependent internal heat source/sink. *Appl. Appl. Math.* **2015**, *10*, 20.
19. Khan, W.A.; Pop, I.M. Boundary layer flow past a stretching surface in a porous medium saturated by a nanofluid: Brinkman-Forchheimer model. *PLoS ONE* **2012**, *7*, e47031. [CrossRef]
20. Alam, A.; Marwat, D.N.K.; Ali, A. Flow of nano-fluid over a sheet of variable thickness with non-uniform stretching (shrinking) and porous velocities. *Adv. Mech. Eng.* **2021**, *13*, 1–16. [CrossRef]
21. Uddin, M.J.; Khan, W.A.; Amin, N.S. g-Jitter mixed convective slip flow of nanofluid past a permeable stretching sheet embedded in a Darcian porous media with variable viscosity. *PLoS ONE* **2014**, *9*, e99384. [CrossRef]
22. Jafar, A.B.; Shafie, S.; Ullah, I. MHD radiative nanofluid flow induced by a nonlinear stretching sheet in a porous medium. *Heliyon* **2020**, *6*, e04201. [CrossRef]
23. Prasannakumara, B.C.; Shashikumar, N.S.; Venkatesh, P. Boundary layer flow and heat transfer of fluid particle suspension with nanoparticles over a nonlinear stretching sheet embedded in a porous medium. *Nonlinear Eng.* **2017**, *6*, 179–190. [CrossRef]
24. Narender, G.; Misra, S.; Govardhan, K. Numerical Solution of MHD Nanofluid over a Stretching Surface with Chemical Reaction and Viscous Dissipation. *Chem. Eng. Res. Bull.* **2019**, *21*, 36–45. [CrossRef]
25. Dessie, H.; Fissha, D. MHD Mixed Convective Flow of Maxwell Nanofluid Past a Porous Vertical Stretching Sheet in Presence of Chemical Reaction. *Appl. Appl. Math.* **2020**, *15*, 31.
26. Gireesha, B.J.; Mahanthesh, B.; Manjunatha, P.T.; Gorla, R.S.R. Numerical solution for hydromagnetic boundary layer flow and heat transfer past a stretching surface embedded in non-Darcy porous medium with fluid-particle suspension. *J. Niger. Math. Soc.* **2015**, *34*, 267–285. [CrossRef]
27. Lakshmi, K.K.; Gireesha, B.J.; Gorla, R.S.; Mahanthesh, B. Effects of diffusion-thermo and thermo-diffusion on two-phase boundary layer flow past a stretching sheet with fluid-particle suspension and chemical reaction: A numerical study. *J. Niger. Math. Soc.* **2016**, *35*, 66–81. [CrossRef]
28. Krishna, M.V.; Chamkha, A.J. Hall and ion slip effects on MHD rotating boundary layer flow of nanofluid past an infinite vertical plate embedded in a porous medium. *Results Phys.* **2019**, *15*, 102652. [CrossRef]
29. Gireesha, B.J.; Mahanthesh, B.; Gorla, R.S.R. Suspended particle effect on nanofluid boundary layer flow past a stretching surface. *J. Nanofluids* **2014**, *3*, 267–277. [CrossRef]
30. Maranna, T.; Sneha, K.N.; Mahabaleshwar, U.S.; Sarris, I.E.; Karakasidis, T.E. An Effect of Radiation and MHD Newtonian Fluid over a Stretching/Shrinking Sheet with CNTs and Mass Transpiration. *Appl. Sci.* **2022**, *12*, 5466. [CrossRef]
31. Mabood, F.; Fatunmbi, E.O.; Benos, L.; Sarris, I.E. Entropy Generation in the Magnetohydrodynamic Jeffrey Nanofluid Flow Over a Stretching Sheet with Wide Range of Engineering Application Parameters. *Int. J. Appl. Comput. Math.* **2022**, *8*, 98. [CrossRef]
32. Baranovskii, E.S. Flows of a polymer fluid in domain with impermeable boundaries. *Comput. Math. Math. Phys.* **2014**, *54*, 1589–1596. [CrossRef]
33. Kakac, S.; Yener, Y. *Convective Heat Transfer*; CRC Press: Boca Raton, FL, USA, 1995; pp. 312–314, 399.